Constitutive model for reinforced concrete

CONSTITUTIVE MODEL FOR REINFORCED CONCRETE

By Peter H. Feenstra[1] and René de Borst[2]

ABSTRACT: A numerical model is proposed for reinforced-concrete behavior that combines some commonly accepted ideas for modeling plain concrete, reinforcement, and interaction behavior (e.g., due to bond) in a consistent manner. The basic idea is that the total stress that exists in a reinforced-concrete element can be rigorously decomposed into individual contributions of the plain concrete, the reinforcement, and the interaction between these constituents. The behavior of plain concrete is governed by fracture-energy–based formulations both in tension and in compression. In this fashion, mesh-independent results can be obtained with respect to the limit load. In the presence of reinforcement, the fracture energy is assumed to be distributed over a tributary area that belongs to a crack. The crack spacing is estimated using accepted CEB-FIP recommendations. The reinforcement is modeled using a standard elastoplastic model, and for the stress contribution that results from the interaction between concrete and reinforcement a trilinear function is adopted. Although the model allows for inclusion of dowel action, this contribution proved unimportant in the structures considered. The application of the model to reinforced-concrete panels and shear walls gives good simulations of the failure behavior.

INTRODUCTION

In spite of more than two decades of research, numerical predictions of the failure behavior of reinforced-concrete structures still show a considerable scatter. Often the failure load and the ductility of reinforced-concrete structures can only be computed accurately by tuning material or system parameters to the specific structure, as was made clear in the early 1980s in a competition to predict experiments by Vecchio and Collins (1982). The lack of reliability in predictions and the fact that the model parameters often have to be adapted to the structure in order to obtain a good agreement with experimental data has motivated the search for improved models for reinforced concrete. An overview of developments since then can be found in the recent ASCE state-of-the-art text (Isenberg 1993). In this contribution, a transparent phenomenological model of reinforced concrete is developed, which combines accepted ideas for modeling the separate features of reinforced-concrete behavior in a consistent fashion. It should also give accurate predictions of the mechanical behavior of reinforced-concrete structures, utilizing robust numerical tools. By the word "accurate," we mean that the accuracy of the numerical predictions should be in the same order as the scatter that is inherent in experimental data of concrete structures.

In this contribution we outline a phenomenological model for reinforced-concrete behavior that unifies some by now established concepts for particulate phenomena like tension-softening and uses accepted guidelines, e.g., the Comité Euro-International du Béton–Federation Internationale de la Precontrainte (CEB-FIP) model code (CEB-FIP 1990). The fundamental assumption is that the total stress in a reinforced-concrete element consists of the contributions of both constituents, concrete and reinforcement, and a so-called interaction stress contribution, which incorporates effects like possible dowel action and tension-stiffening. In the literature, the tension-stiffening effect is usually referred to as the ability to gradually redistribute the load in a structure from concrete to steel under the formation of primary and secondary cracks. In our approach, the tension-stiffening effect is conceived as the additional stiffness due to the interaction between concrete and reinforcement in the direction of the reinforcement; the formation of primary and secondary cracks is modeled with the constitutive model of plain concrete in tension, the tension-softening model. In the presence of reinforcement, the fracture energy in this model is distributed over a tributary area by using the crack spacing as formulated in the CEB-FIP (1990) model code, thus ensuring finite-element discretization-independent results.

This contribution is organized as follows. First, the assumption of the stress decomposition is detailed. Then, the various stress contributions are discussed. The tension-softening model for plain concrete is outlined including its use in smeared-crack finite-element analyses and a rational extension to reinforced-concrete behavior. A fracture-energy–based model for concrete in compression is proposed, and the modeling of the reinforcement and interaction stresses are detailed. Then, the proper choice of a smeared-crack model is treated in the light of the rotation of the principal axes of stress and strain, which inevitably occurs in reinforced-concrete structures. Finally, the adopted philosophy for the tension-stiffening model is systematically validated using a number of reinforced-concrete panels, and some applications are made to reinforced shear walls to demonstrate the versatility of the model.

GENERAL FRAMEWORK

In this study, it is assumed that the behavior of cracked reinforced concrete can be obtained by superposition of the stiffness of plain concrete, a stiffness of the reinforcement, and an additional stiffness due to interaction between concrete and reinforcement. This leads to the following summation of stress contributions:

$$\boldsymbol{\sigma} = \boldsymbol{\sigma}_c + \boldsymbol{\sigma}_s + \boldsymbol{\sigma}_{ia} \tag{1}$$

where $\boldsymbol{\sigma}_c$ = stress contribution of the plain concrete; σ_s = contribution of the reinforcing steel; and $\boldsymbol{\sigma}_{ia}$ = interaction stress contribution due to tension-stiffening [see also Fig. 1(a)].

Behavior of Plain Concrete

The constitutive behavior of concrete will be modeled with a smeared model where the damaged material is considered to be a continuum in which the notions of stress and strain apply. Consequently, the damage is also considered distributed and it is assumed that the damage can be represented

[1]Res. Engr., Delft Univ. of Technol., Dept. of Civ. Engrg., P.O. Box 5048, 2600 GA Delft, The Netherlands.
[2]Prof., Delft Univ. of Technol., Dept. of Civ. Engrg., P.O. Box 5048, 2600 GA Delft, The Netherlands.

Note. Associate Editor: Jean-Lou A. Chameau. Discussion open until October 1, 1995. To extend the closing date one month, a written request must be filed with the ASCE Manager of Journals. The manuscript for this paper was submitted for review and possible publication on March 8, 1994. This paper is part of the *Journal of Engineering Mechanics*, Vol. 121, No. 5, May, 1995. ©ASCE, ISSN 0733-9399/95/0005-0587–0595/ $2.00 + $.25 per page. Paper No. 7960.

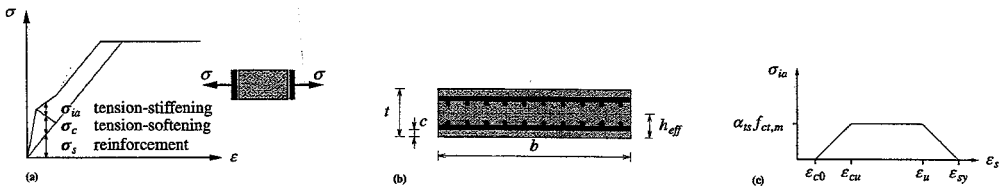

FIG. 1. (a) Idealized Representation of Constitutive Model of Reinforced Concrete; (b) Effective Tension Area in Concrete Slab with Two Reinforcement Layers (CEB-FIP 1990); (c) Tension-Stiffening Diagram

by two internal parameters, κ_T in tension and κ_C in compression. These internal parameters are related to the released energy per unit damaged area by an equivalent length h. For tensile cracking, the concept of the fracture energy G_f and an equivalent length, or crack band width, has extensively been used in finite-element calculations. In this fashion, the results that are obtained with a finite-element analysis are objective with respect to mesh refinement (de Borst 1986). In this study, this concept of released energy and equivalent length is also proposed to model the compressive softening behavior by introducing a compressive fracture energy G_c and using the equivalent length h. However, it is recognized that the underlying failure mechanisms in compression may be more related to the volume of the elements than to a representative length of the elements.

In finite-element calculations the equivalent length corresponds to a representative dimension of the mesh size, as pointed out by many authors [see Bažant and Oh (1983), Willam (1984), Rots (1988), and Oliver (1989)]. The equivalent length at least depends on the chosen element type, element size, element shape, and the integration scheme. In this study, it is assumed that the equivalent length can be related to the area of an element as follows:

$$h = \alpha_h \sqrt{A_e} = \alpha_h \left[\sum_{\xi=1}^{n_\xi} \sum_{\eta=1}^{n_\eta} \det(\mathbf{J}) w_\xi w_\eta \right]^{1/2} \tag{2}$$

in which w_ξ and w_η = weight factors of the Gaussian integration rule because it is tacitly assumed that the elements are integrated numerically. The local, isoparametric coordinates of the integration points are given by ξ and η; and $\det(\mathbf{J})$ = Jacobian of the transformation between the local, isoparametric coordinates and the global coordinate system. The factor α_h = a modification factor that is equal to 1 for quadratic elements and equal to $\sqrt{2}$ for linear elements (Rots 1988). For most practical applications the formulation for the equivalent length, (2) gives a good approximation.

The experiments of Kupfer and Gerstle (1973) for plain concrete subjected to proportional biaxial loading have been used to define a composite failure surface with a von Mises–type yield contour in the compression-compression regime and the principal-stress-failure condition of Rankine in the tensile regime, i.e.

$$f_C = \sqrt{3J_2} - \bar{\sigma}_C(\kappa_C) \tag{3a}$$

$$f_T = \sigma_1 - \bar{\sigma}_T(\kappa_T) \tag{3b}$$

where J_2 = second invariant of the stresses; and σ_1 = major principal stress. The constitutive behavior is then completely governed by the equivalent stress functions, $\bar{\sigma}_C(\kappa_C)$ and $\bar{\sigma}_T(\kappa_T)$ as a (non)linear function of the internal parameters κ_C and κ_T, respectively. Further details about the composite plasticity model are given in Feenstra (1993).

The compressive stress-strain behavior can be approximated by different functions [e.g., Vecchio and Collins (1982) and CEB-FIP (1990)], but these relations are usually not energy–based formulations. In this study, the behavior in compression will be modeled with a compression-softening model as defined by the following parabolic equivalent stress–equivalent strain diagram:

$$\bar{\sigma}_C(\kappa_C) = \frac{f_{cm}}{3}\left(1 + 4\frac{\kappa_C}{\kappa_e} - 2\frac{\kappa_C^2}{\kappa_e^2}\right), \quad \text{if } \kappa_C < \kappa_e \tag{4a}$$

$$\bar{\sigma}_C(\kappa_C) = f_{cm}\left[1 - \frac{(\kappa_C - \kappa_e)^2}{(\kappa_{uC} - \kappa_e)^2}\right], \quad \text{if } \kappa_e \le \kappa_C < \kappa_{uC} \tag{4b}$$

where κ_C = an internal damage parameter; and f_{cm} = mean value of the compressive strength. The maximum compressive strength will be reached at an equivalent strain κ_e, which is independent of the element size h and reads as follows:

$$\kappa_e = \frac{4f_{cm}}{3E_c} \tag{5}$$

where E_c = Young's modulus of the concrete, which has been assumed to be given by CEB-FIP (1990) model code regulations. The maximum equivalent strain κ_u is related to the compressive fracture energy G_c and the element size h and reads as follows:

$$\kappa_{uC} = 1.5\frac{G_c}{hf_{cm}} \tag{6}$$

The compressive fracture energy G_c is assumed to be a material parameter for which experimental data has been provided by Vonk (1992).

In reinforced concrete, the compressive strength of the plain concrete is usually reduced because it is assumed that the compressive strength of plain concrete is affected by cracking in the lateral direction (Vecchio and Collins 1982). After a careful examination of recent experimental data by Kollegger and Mehlhorn (1990a), Feenstra (1993) concluded that a reasonable approximation is to reduce the compressive strength of reinforced concrete in biaxial tension-compression by a constant factor of 20%. This proposal has also been followed in this study.

The tensile stress-strain relationship can be approximated by different functions [e.g., CEB-FIP (1990) and Hordijk (1991)]. In this study, a linear softening diagram will be used, which is sufficiently accurate for the envisaged class of applications (reinforced-concrete panels and shear walls, plates, and shells). The equivalent stress as a function of the internal damage parameter κ_T is then given by the following:

$$\bar{\sigma}_T(\kappa_T) = f_{ct,m}\left(1 - \frac{\kappa_T}{\kappa_{uT}}\right) \tag{7}$$

and the ultimate damage parameter κ_{uT} reads as follows:

$$\kappa_{uT} = \frac{2G_f}{hf_{ct,m}} \tag{8}$$

The tensile strength of concrete $f_{ct,m}$ has been related to the compressive strength f_{cm}, in accordance with the CEB-FIP (1990) model code. The fracture energy in tension, G_f, is assumed to be a material parameter and has been related to

the compressive strength of the material f_{cm} and the maximum aggregate size d_{max}, according to the CEB-FIP (1990) model code.

By introducing the concept of an equivalent length, the ultimate internal parameters, and thus the equivalent stress-strain diagrams, depend on the element size. Both ultimate internal parameters, κ_{uC} and κ_{uT}, are assumed constant during the analysis and are considered to be element-related material parameters since they can be calculated from the material properties (the ultimate strength and the fracture energy) and the element area represented by the equivalent length.

Behavior of Reinforced Concrete

In reinforced concrete, usually a number of cracks develop during the process of loading until the cracking process stabilizes and no further cracks develop in the structure. The crack spacing at stabilized cracking is determined mainly by the amount of reinforcement. It is assumed in this study that the material model for plain concrete, based on fracture energy, can be applied to reinforced concrete, with the total amount of fracture energy dissipated over the equivalent length. Because the fracture energy is assumed to be a material parameter, only the average crack spacing has to be determined.

The total amount of released energy at stabilized cracking is determined by the fracture energy of a single crack G_f and the average crack spacing l_s. In general, the dimensions of the finite elements in simulations of reinforced-concrete structures, and thus the equivalent length h, are much larger than the average crack spacing l_s, and therefore it is assumed that the released energy can be determined by the following:

$$G_f^c = \min\left\{G_f,\ G_f\frac{h}{l_s}\right\} \tag{9}$$

where G_f = fracture energy of a single crack; h = equivalent length; and l_s = average crack spacing. If the equivalent length h is smaller than the average crack spacing l_s, the model will result in an overestimation of the released fracture energy and, consequently, a too-stiff behavior. The average crack spacing is a function of the bar diameter, the concrete cover, and the reinforcement ratio according to the CEB-FIP model code (1990), which reads as follows:

$$l_s = \frac{2}{3}l_{s,\max} = \frac{2}{3}\left(2s_0 + \frac{\phi_s}{\gamma\rho_s}\right) \tag{10}$$

where s_0 = minimum bond length; ϕ_s = diameter of the reinforcement; a factor $\gamma = 4$ for deformed bars and $\gamma = 2$ for plain bars; and the reinforcement ratio ρ_s given by the following:

$$\rho_s = \frac{A_s}{A_c} \tag{11}$$

where A_s = total area of reinforcement; and A_c = cross area of the tensile member. The minimum bond length s_0 is usually taken equal to 25 mm in the absence of more precise data. A comparison of 132 experiments on tensile members (Braam 1990), showed that the average crack spacing given by (10) is a good approximation of the experimentally observed crack spacing.

Now, attention will be focused on the approximation of the released energy in plane two-dimensional structures like panels, reinforced with a reinforcing grid in two orthogonal directions. The crack spacing in panels is usually determined by treating a panel as a tensile member by the definition of an effective reinforcement ratio. If the reinforcement is supplied with a layer of a reinforcing grid, the average crack spacing is calculated with a modified expression of (10), as follows:

$$l_s = \frac{2}{3}l_{s,\max} = \frac{2}{3}\left(2s_0 + \frac{\phi_s}{\alpha\rho_{s,eff}}\right) \tag{12}$$

with the effective reinforcement ratio $\rho_{s,eff}$ determined by the following:

$$\rho_{s,eff} = \frac{A_s}{A_{c,eff}} \tag{13}$$

The effective tension area, $A_{c,eff} = h_{eff}b$, is estimated according to the CEB-FIP (1990) recommendations with the following relation:

$$h_{eff} = \min\left[2.5\left(c + \frac{\phi_{eq}}{2}\right), \frac{t}{2}\right]$$

where c = concrete cover on the reinforcement; ϕ_{eq} = equivalent bar diameter of the reinforcement; and t = thickness of the structure. These geometrical properties are shown in Fig. 1(b). The effective tension area is calculated with the equivalent bar diameter of the reinforcing grid, which is determined by the following:

$$\phi_{eq} = \frac{\phi_p\rho_p + \phi_q\rho_q}{\rho_p + \rho_q} \tag{14}$$

with the reinforcement ratios ρ_p and ρ_q in the p- and q-directions of the reinforcing grid, respectively. The diameter of the reinforcement is given by ϕ_p and ϕ_q in the p- and q-direction. The average crack spacing can now be calculated in the two directions of the reinforcing grid. The crack spacing given by (12) is based on the fact that the cracks form at right angles to the reinforcing direction. When the cracks form at inclined angles with the reinforcing directions this identity cannot be used to estimate the crack spacing. Then, the average crack spacing is calculated with the following expression (CEB-FIP 1990):

$$l_s = \left(\frac{|\cos\alpha|}{l_{s,p}} + \frac{|\sin\alpha|}{l_{s,q}}\right)^{-1} \tag{15}$$

where α = angle between the reinforcement in the p-direction and the direction of the principal tensile stress at incipient cracking. The crack spacings predicted with (15) are theoretically reasonable. For a structure reinforced equally in the p- and q-directions subjected to a pure shear loading, the cracks are forming at 45° to the p-direction and the crack spacing is $1/2\sqrt{2}$ times the crack spacing in the p- or q-direction. If the structure is only reinforced in the p-direction, the crack spacing for tension in the p-direction is equal to the value given by (12). For tension in the q-direction the predicted crack spacing is equal to infinity, which implies that only one crack is formed in the structure. Comparison of the theoretical crack spacing with the experimental results of structures reinforced in one directional shows that the trend of the crack spacing with increasing angle α is predicted correctly, but that the crack spacing is usually underestimated (Bhide and Collins 1987). This is because only primary cracks have been observed, with the secondary cracks being ignored. The expression of (15) may be used according to the CEB-FIP (1990) model code when a more advanced model is not available.

As indicated in Fig. 1(b), the reinforcement is usually applied in more layers with different directions through the thickness of the structure. The average crack spacing of the structure is then determined by the smallest average crack spacing of all reinforcing grids. The average crack spacing in the case of different reinforcing grids with arbitrary directions will be given by a modification of (15), as follows:

$$l_s = (a_x + a_y)^{-1} \tag{16}$$

in which the factors a_x and a_y are determined by the following:

$$a_x = \max\left(\frac{|\cos\alpha_j|}{l_{s,pj}}\right) \tag{17a}$$

and

$$a_y = \max\left(\frac{|\sin\alpha_j|}{l_{s,qj}}\right), \text{ for } j = 1, \ldots, n_{\text{grid}} \tag{17b}$$

where α_j = angle between the reinforcement p-direction and the direction of the principal tensile stress at incipient cracking. It has tacitly been assumed that the cracks propagate through the entire thickness of the structure with no localization in the thickness direction. With this approach, the fracture energy in reinforced concrete can be assessed on the basis of the fracture energy of concrete, the reinforcement properties, and the angle between reinforcement and the principal stress at incipient cracking. In this fashion, the tension-softening of reinforced concrete has been formulated in a rational fashion.

Modeling of Reinforcement

The constitutive model of the reinforcement is assumed to be given by an elastoplastic model with a stiffness matrix given by the following:

$$\mathbf{D}_s = \begin{bmatrix} \rho_p E_s^{ep} & 0 & 0 \\ 0 & \rho_q E_s^{ep} & 0 \\ 0 & 0 & 0 \end{bmatrix} \tag{18}$$

in which ρ_p and ρ_q = reinforcement ratios in the p- and q-directions, respectively; and E_s^{ep} = elastoplastic modulus of the reinforcement. The shear stiffness of the reinforcing grid is assumed to be equal to zero. The stress contribution in the global x, y-coordinate system is computed via the following:

$$\boldsymbol{\sigma}_s = [\mathbf{T}^T(\psi)\mathbf{D}_s\mathbf{T}(\psi)]\boldsymbol{\varepsilon} \tag{19}$$

where $\boldsymbol{\varepsilon}$ = strain vector in the global x, y-coordinate system; and $\mathbf{T}(\psi)$ = standard transformation matrix between two coordinate systems, with ψ = angle between the x-axis and the main reinforcement p-axis.

Interaction Stress Contribution

After a stabilized crack pattern has developed, stresses are still transferred from reinforcement to concrete between the cracks due to the bond action, which increases the total stiffness of the structure [Fig. 1(a)]. The additional stress due to tension-stiffening is assumed to be given as a function of the strain in the direction of the reinforcement and will be active on the effective tension area defined in Fig. 1(b). The interaction stress is assumed to be given by a trilinear function according to Cervenka et al. (1990), as depicted in Fig. 1(c). The interaction stress is only active if the strain in the reinforcement is larger than ε_{c0}, which is determined by the following:

$$\varepsilon_{c0} = \frac{f_{ct,m}}{E_c}\cos^2\alpha \tag{20}$$

where α = angle between the direction of the reinforcement and the direction of the principal stress at incipient cracking. The factor ε_{cu} is determined by the crack spacing, the equivalent length of the element, and the fracture energy of the concrete, and is given by the following:

$$\varepsilon_{cu} = 2\cos^2\alpha\,\frac{G_f^{fc}}{hf_{ct,m}} \tag{21}$$

The constant part of the diagram is a fraction of the tensile strength of the concrete with the factor α_{ts} as a rough approximation equal to the tensile strength, i.e., $\alpha_{ts} = 1.0$. The tension-stiffening component is reduced near the yield strain of the reinforcement ε_{sy} in order to avoid an artificial increase of the yield stress of the reinforcement. The strain at which the tension-stiffening component is reduced is given by the following:

$$\varepsilon_u = \varepsilon_{sy} - \frac{\alpha_{ts}f_{ct,m}}{\rho_{s,eff}E_s} \tag{22}$$

The local stiffness matrix that incorporates the interaction stiffness is then given by the following:

$$\mathbf{D}_{ia} = \begin{bmatrix} E_{b,p} & 0 & 0 \\ 0 & E_{b,q} & 0 \\ 0 & 0 & 0 \end{bmatrix} \tag{23}$$

in which $E_{b,p}$ and $E_{b,q}$ = bond stiffnesses in the p- and q-directions of the grid, respectively. The transformation to the global coordinate system again follows from

$$\boldsymbol{\sigma}_{ia} = [\mathbf{T}^T(\psi)\mathbf{D}_{ia}\mathbf{T}(\psi)]\boldsymbol{\varepsilon} \tag{24}$$

SMEARED-CRACK MODEL FOR CONCRETE IN TENSION

In smeared-crack analyses of plain- and reinforced-concrete structures, a major issue has been the proper choice of the smeared-crack concept in which the tension-softening model discussed before is embedded. In the first smeared-crack model by Rashid (1968), the major principal stress was set equal to zero immediately upon violation of the tensile strength of the concrete. Also the shear capacity in this direction was assumed to have vanished, and a zero shear stiffness was inserted in the anisotropic elastic stress-strain relation. Later, enhancements were proposed, such as the partial retention of shear stiffness across the crack face via a shear-retention factor (Suidan and Schnobrich 1973) and the tension-softening model. A consequence of the introduction of a shear-retention factor and a softening branch is that the principal stress axes rotate after incipient cracking and cease to coincide with the normal to the crack. Indeed, the major principal stress may even exceed the tensile strength in another direction. Neglecting this effect causes spurious stresses to occur and tends to result in collapse loads that severely overestimate the true failure load. Different proposals have been suggested to improve the behavior of the standard fixed-crack approach, like the rotating-crack model [cf. Rots (1988)], or a deformation plasticity model with a Rankine (principal stress) yield criterion (Crisfield and Wills 1989; Feenstra 1993).

Now, we shall investigate whether the improvements of these classes of models reported for plain concrete also pertain to reinforced-concrete elements. This will be done using an idealized panel proposed by Crisfield and Wills (1989). The analysis concerns a single element, dimensions 10 × 10 mm² with a thickness of 1 mm, reinforced with one layer of a reinforcing grid with $\psi = 0°$ (Fig. 2). The reinforcement ratio in the p-direction is equal to 0.04232 and in the q-direction equal to 0.00768. A no-tension analysis is carried out

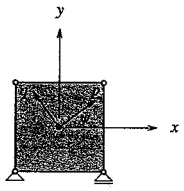

FIG. 2. Finite-Element Model of Reinforced-Concrete Panels

with linear-elastic behavior in compression (Young's modulus E = 20,000 MPa), which results in a limit analysis with an exact failure load. The Young's modulus of the reinforcement is E_s = 200,000 MPa, and the yield strength of the steel is f_{sy} = 500 MPa. The panel is loaded in a combined biaxial tension-shear loading with $f_{xx} = f_{yy} = 2.5\mu$ MPa and $f_{xy} = 5.0\mu$ MPa, with μ = loading parameter such that it is equal to one at the exact collapse load associated with yielding of the reinforcement (Crisfield and Wills 1989).

The results of the analyses are shown in Fig. 3, where the loading parameter is plotted against the x-displacement of the upper-right node of the element. The comparison of the different smeared-crack formulations for plain concrete shows that a proper choice is important even if the tensile strength is equal to zero and no tension-softening description is used. The interaction between the reinforcement and the concrete compressive struts after cracking results in different responses. The fixed-crack model shows a collapse load that is too high, irrespective of the magnitude of the shear-retention factor. The rotating-crack model and the plasticity-based models approximate the exact failure load. The responses of the rotating-crack model and the Rankine plasticity model based on a deformation theory are identical [cf. Crisfield and Wills (1989)].

A deficiency of a total formulation like the rotating-crack model is that a transparent combination with other nonlinear phenomena is difficult. The deformation plasticity model utilizing the Rankine (principal stress) yield criterion suffers from the drawback that it is difficult to incorporate local unloading in this model. As has been shown by Feenstra (1993), the Rankine plasticity model with an incremental formulation shows a behavior that is very similar to the behavior of the rotating-crack model. Because a robust numerical algorithm can be developed for this model, it will be used in the example calculations.

VALIDATION OF TENSION-STIFFENING MODEL

The interaction model has been validated with experiments on reinforced-concrete panels subjected to in-plane shear and normal loading. All panels are 890 × 890 mm² with a thickness of 70 mm, reinforced with two layers of a reinforcing grid. The cover of the reinforcing grids is equal to 6 mm for all panels that have been analyzed. The finite-element idealization for the analyses consists of a four-noded element with four integration points for both the reinforcement and the concrete (Fig. 2). The reinforcement in the panels is represented by the angle ψ between element x-axis and main reinforcement p-axis and the reinforcement ratios in p- and q-directions.

The first analyses concern experiments for which the loading regime and the properties of the reinforcement are designed such that no rotation of the principal strain occurs after cracking. Only the model that describes the tension-stiffening effect is utilized, and possible dowel action is not activated.

For the validation of the tension-stiffening model, two panels of Bhide and Collins (1987), panels pb13 and panel pb25, have been selected. Both panels have approximately the same material properties, but the reinforcement ratio of panel pb25 is twice that of panel pb13. The panels are both loaded in uniaxial tension in the direction of the reinforcement. The reinforcement in panel pb13 is applied in two grids with a reinforcement ratio given by ρ_p = 0.01085 and ρ_q = 0.0 and an angle ψ = 0°. The diameter of the deformed bars ϕ_p is equal to 6.55 mm. The mean compressive strength of the concrete has been taken from the report of Bhide and Collins (1987), f_{cm} = 23.4 MPa, and using the CEB-FIP (1990) model code, the Young's modulus of the concrete E_c, the characteristic value of the tensile strength $f_{ct,m}$, and the fracture energy G_f were estimated as E_c = 26,000 MPa, $f_{ct,m}$ = 1.85 MPa, and G_f = 0.06 N/mm, respectively. For concrete, the Poisson ratio ranges from 0.1 to 0.2. In this and the subsequent example calculations a value 0.15 has been adopted. The reinforcement data were E_s = 210,000 MPa and f_{sy} = 414 MPa for the Young's modulus and the yield strength, respectively.

The effective tension area determined by the geometrical properties of the reinforcement is equal to 23.2 mm and the average crack spacing is equal to 100 mm. Compared with the experimental stabilized crack spacing of approximately 111 mm, the calculated value of the average crack spacing is reasonably accurate. The nominal tensile stress-strain diagram of panel pb13 is shown in Fig. 4. The influence of the tension-stiffening component in the constitutive model is obvious from this diagram. The calculated force at cracking of the panel is too high, which indicates that the tensile strength of the concrete is overestimated. This also influences the tension-stiffening effect, which has been chosen with a value equal to one.

Panel pb25 has been designed to study the effect of the amount of reinforcement, and this panel is the companion specimen of panel pb13. The reinforcement ratio of panel pb25 is twice the reinforcement ratio of panel pb13, i.e., ρ_p = 0.02170 with the same angle ψ = 0° and a diameter ϕ_p = 6.59 mm. The reinforcement in the q-direction is again equal to zero. The material parameters for panel pb25 have the same values as those for panel pb13, but for the fact that now the mean value of the compressive strength is given by f_{cm} = 20.0 MPa. The effective tension area determined by the geometrical properties of the reinforcement is again equal to 23.2 mm, and the average crack spacing is equal to 66.5 mm. Compared with the experimental crack spacing of approximately 81 mm, the calculated value of the average crack spacing is quite accurate. The nominal tensile stress-strain diagram

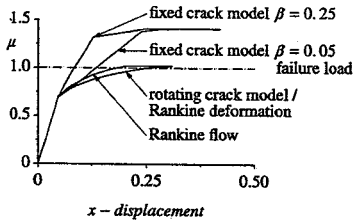

FIG. 3. Results for Idealized Reinforced Concrete Panel

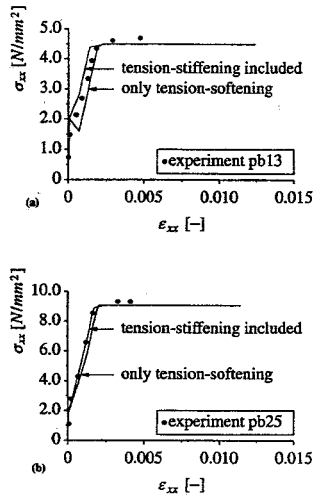

FIG. 4. Influence of Tension-Stiffening on Panels Bhide and Collins (1987): (a) pb13; (b) pb25

of panel pb25 is shown in Fig. 4. It is obvious from this diagram that the tension-stiffening component is less dominant for this panel than for panel pb13.

The influence of the angle between a crack and the reinforcement has been studied with the analyses of two panels tested by Kollegger (1988). It concerns two panels with the same material properties and equal reinforcement, but with a different reinforcement angle ψ. Panel pk03 has an angle ψ equal to 0°, whereas panel pk04 has an angle 45°. The mean value of the compressive strength is equal to $f_{cm} = 20.0$ MPa, and the derived material parameters are $E_c = 26{,}000$ MPa, $f_{ct,m} = 1.6$ MPa, and $G_f = 0.06$ N/mm.

The reinforcement data were $E_s = 210{,}000$ MPa and $f_{sy} = 700$ MPa, respectively. The reinforcement ratio in the p- and q-direction is equal to 0.0106 with a diameter of 6.5 mm. The effective tension area is equal to 23.1 mm, the average crack spacing is equal to 100 mm for panel pk03, and the average crack spacing is equal to 70 mm for panel pk04, which is in agreement with the experimental value of the stabilized crack spacing. The nominal stress-strain response in the x-direction of panels pk03 and pk04 has been depicted in Fig. 5.

The assumption that the tension-stiffening component acts in the direction of reinforcement is supported by the analyses of the panels, which show that the calculated behavior is close to the experimental behavior. The conclusion of Kollegger and Mehlhorn (1990b) that the influence of the angle between crack and reinforcement is negligible for the tension-stiffening model is confirmed by these analyses.

The following analyses will concern reinforced panels of Vecchio and Collins (1982), which are anisotropically reinforced. Due to this anisotropy, the direction of the principal strain will change after crack initiation. The degree of anisotropy is defined by the ratio of the potential yield loads of the reinforcement (Crisfield and Wills 1989), as follows:

$$\omega_r = \frac{\rho_p f_{sy,p}}{\rho_p f_{sy,q}} \tag{25}$$

The first panel concerns panel pv10 with a moderate anisotropy factor $\omega_r = 1.79$. The reinforcement ratio in the p-direction is equal to 0.01785 with a diameter of 6.35 mm, and in the q-direction equal to 0.00999 with a diameter of 4.70 mm. This results in an effective tension area of 22.9 mm in the p-direction and 20.8 mm in the q-direction. The average crack spacing is equal to 51.4 mm, which is in agreement with the experimentally observed crack spacing of 50–75 mm. The values of the relevant material parameters for the concrete are $E_c = 24{,}000$ MPa; $f_{cm} = 14.4$ MPa; $f_{ct,m} = 1.0$ MPa; and $G_f = 0.06$ N/mm. The steel properties are $E_s = 210{,}000$ MPa and $f_{sy} = 276$ MPa.

The nominal shear stress–shear strain response is given in Fig. 6. The comparison of the analysis with the experiment shows that the tensile strength is underestimated, but that the agreement is reasonable. The influence of the tension-stiffening component is small because the ultimate crack strain is almost equal to the failure strain of the element.

The second panel that has been analyzed is pv12, which has a large anisotropy factor $\omega_r = 6.98$. This large anisotropy factor produces a significant change in the principal strain directions. The reinforcement is applied in two layers of reinforcing grids with a reinforcement ratio in the p-direction equal to 0.01785 with a diameter of 6.35 mm, and in the q-direction equal to 0.00446 with a diameter of 3.18 mm. These properties result in an effective tension area of 22.4 mm. The average crack spacing is equal to 51.4 mm, which is in agreement with the experimentally observed crack spacing of 50–75 mm.

The yield stress of the reinforcing steel is different in the p- and q-directions, because $f_{sy,p} = 469$ MPa, and $f_{sy,q} = 269$ MPa. The mean compressive strength of the concrete is slightly higher than for the panel pv10, $f_{cm} = 16.0$ MPa, and accordingly $E_c = 25{,}000$ MPa and $f_{ct,m} = 1.2$ MPa. The other parameters for concrete and reinforcement are the same as for panel pv10. The nominal shear stress–shear strain response is given in Fig. 6. It is evident from the results for panel pv12 that the shear resistance of the cracked reinforced concrete becomes more important if the directions of the principal strain vector change significantly. However, the ultimate failure load is not affected if the failure mode is governed by yielding of the reinforcement.

It is assumed that neglecting the shear resistance of the cracked reinforced concrete is allowed as long as the anisotropy of the reinforcement is less than five and the loading is such that rotation of the principal directions can be expected. In cases where the structure is reinforced only in one direction, the Rankine model should be used with care, because the analysis might show a much too brittle response due to continuous rotation of the principal stress axes.

APPLICATION TO REINFORCED-CONCRETE SHEAR WALLS

The analysis of shear-wall panels is a good example of the possible application of the developed models. The stress state in the panels can be considered to be in tension-compression.

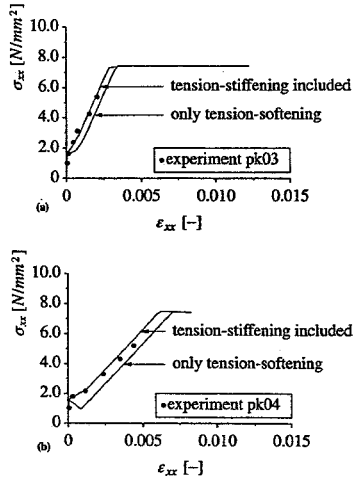

FIG. 5. Influence of Tension-Stiffening on Panels Kollegger (1988): (a) pk03; (b) pk04

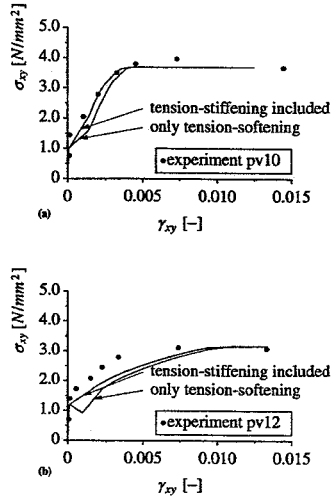

FIG. 6. Influence of Tension-Stiffening on Panels Vecchio and Collins (1982): (a) pv10; (b) pv12

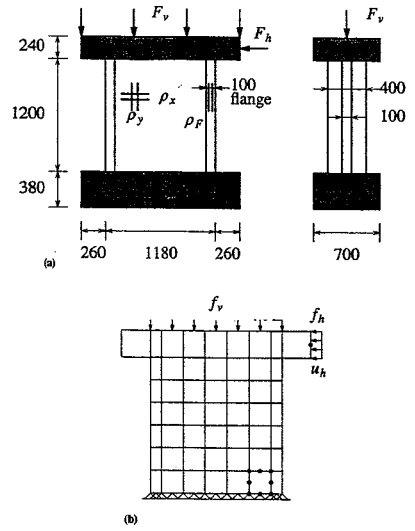

FIG. 7. Panels S1 and S2 of Maier and Thürlimann (1985): (a) Experimental Setup; (b) Finite-Element Discretization

The panels are usually reinforced by a reinforcing grid, which makes the examples also a good indicator for the influence of the tension-stiffening on the behavior of the panels. The panels that will be presented in this study have been tested at the Eidgenössiche Technische Hochschule (ETH) Zürich by Maier and Thürlimann (1985). The experimental program of Maier and Thürlimann (1985) concerned a series of 10 shear-wall panels with flanges and panels without flanges. The panels were all loaded initially by a vertical compressive force, and then loaded by a horizontal force until the experiment became unstable and the failure load had been reached. The experimental setup is shown in Fig. 7, with the panels supported on a base block and loaded through a thick top slab.

From the series, two panels with flanges, S1 and S2, have been analyzed with the composite plasticity model, and the influence of the tension-stiffening component on the behavior has been examined. The material properties have been averaged from the experimental data of four of the ten panels tested by Thürlimann and Maier (1985) with a reduction of the compressive strength of 20%. The mean value of the concrete compressive strength is $f_{cm} = 27.5$ MPa, and the other parameters have been assigned the following values using the CEB-FIP (1990) model code: $E_c = 30{,}000$ MPa; $f_{ct,m} = 2.2$ MPa; $G_f = 0.07$ MPa; and $G_c = 50$ MPa. The Young's modulus of the reinforcement was $E_s = 200{,}000$ MPa, and f_{sy} grows from 574 MPa at initial yield to 764 MPa at a strain level $\varepsilon_{sy} = 24.6 \times 10^{-3}$. These parameters result from an averaging procedure with respect to the material properties in order to simulate the behavior of the panels in a qualitative manner. In this way, it is possible to study the influence of the initial vertical stress on the mechanical behavior.

The reinforcement is applied by reinforcing grids in two directions with a diameter of 8 mm and a clear cover of 10 mm. The reinforcement ratios for both panels are $\rho_x = 10.3 \times 10^{-3}$ for the x-direction; $\rho_y = 11.6 \times 10^{-3}$ for the y-direction; and $\rho_F = 11.6 \times 10^{-3}$ for the flanges. The finite-element discretizations of the panels are depicted in Fig. 7 with quadratic plane-stress elements with a nine-point Gaussian integration for both the reinforcement and the element. The reinforcement has been applied in two layers of a reinforcing grid. The top slab has been modeled with linear-elastic elements without reinforcement, whereas the supporting block has been replaced by fixed supports in the x- and y-directions.

The horizontal and vertical load have been applied as a uniformly distributed element load as indicated in Fig. 7. The horizontal displacement u_h of the top slab has been monitored and compared with the experimental load-displacement curves. Initially, a solution technique with a constrained Newton-Raphson iteration with line searches has been applied to analyze the panels. It happened that it was not possible to achieve converged solutions after the maximum load, and therefore the indirect-displacement-control method (de Borst 1986; Feenstra and Schellekens 1991) without line searches has been used to analyze these panels. The displacement in the horizontal direction u_h has been chosen as the active degree of freedom with load steps of approximately 0.2 mm. With this solution technique, converged solutions could be obtained in the complete loading regime.

Panel S1 is subjected to an initial vertical load of 433 kN $\equiv$ 2.5 N/mm^2, which results in an initial horizontal displacement of 0.06 mm in the experiment. The calculated initial displacement is equal to -80×10^{-6} mm, which indicates a possible eccentricity in the experimental setup. After the ini-

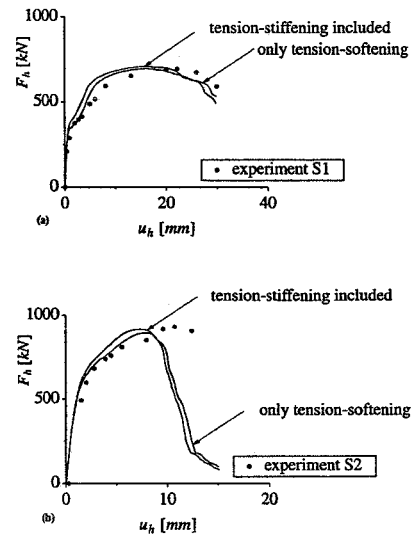

FIG. 8. Load-Displacement Diagrams for Panels Maier and Thürlimann (1985): (a) S1; (b) S2

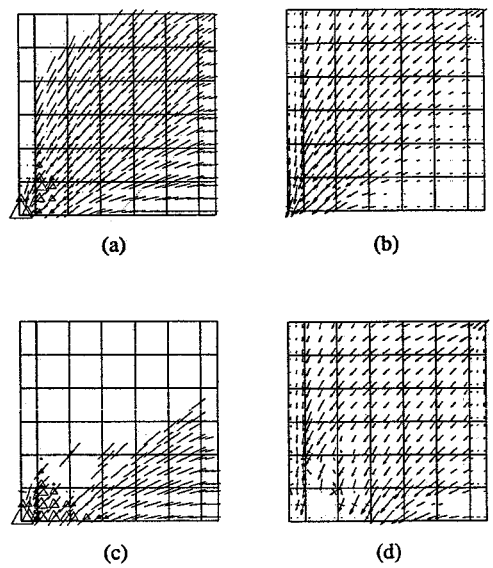

FIG. 9. Finite-Element Results for Panel S1: (a) Active Cracks and Plastic Points at Displacement Level of 10 mm; (b) Principal Stresses at Displacement Level of 10 mm; (c) Active Cracks and Plastic Points at Displacement Level of 30 mm; (d) Principal Stresses at Displacement Level of 30 mm

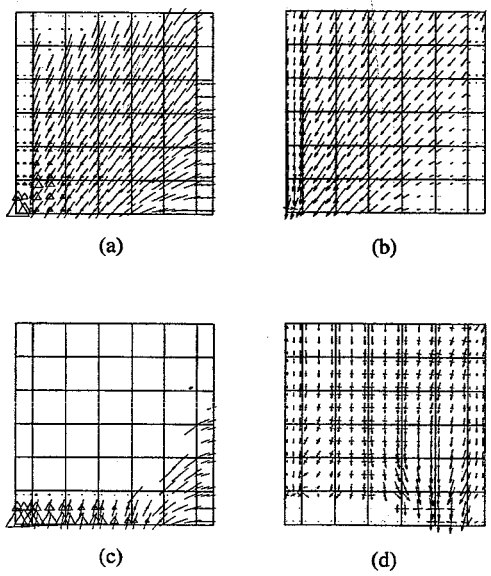

FIG. 10. Finite-Element Results for Panel S2: (a) Active Cracks and Plastic Points at Displacement Level of 5 mm; (b) Principal Stresses at Displacement Level of 5 mm; (c) Active Cracks and Plastic Points at Displacement Level of 15 mm; (d) Principal Stresses at Displacement Level of 15 mm

tial vertical load, the horizontal load is applied with indirect displacement control. The load-displacement diagram of panel S1 is shown in Fig. 8, which shows a reasonable agreement between experimental and calculated response. The influence of the tension-stiffening component on the load-displacement diagram is small, but inclusion of the tension-stiffening avoids some numerical difficulties that are related to local maxima due to crack localization in the prepeak regime. The results of the analysis will be presented by plotting the active cracks as a line; the integration points, which are in a compressive plastic state, as a triangle; and the principal stresses, which are in general compressive, as an arrow. The active cracks are defined as those cracks for which the internal parameter κ_T is equal or greater than 0.5 κ_{uT}. The results for panel S1 at a displacement of the top slab of 10 mm are shown in Fig. 9. The panel is densely cracked with plastic points in the bottom left corner of the panel [Fig. 9(a)]. The concrete in the bottom right corner does not transfer any stress anymore as can be seen from Fig. 9(b). The load-carrying mechanism through a compressive strut can clearly be observed from the principal stresses. The results of panel S1 at the final displacement of 30 mm show the failure mechanism, which is governed by compressive softening of the concrete and yielding of the reinforcing steel both in tension and compression [Fig. 9(c)]. In the ultimate state, the concrete in the bottom left corner transfers no stress anymore [Fig. 9(d)], which is in agreement with the experimentally observed failure mechanism where the concrete was crushed in the bottom left corner of the panel and in the flange at the compression side.

Panel S2 is identical to panel S1 except that the initial vertical load is now 1,653 kN, which increases the ultimate load of the structure but decreases the ductility of the panel significantly (Fig. 8). The agreement between the ultimate load of the experiment and the calculated maximum load is good. The influence of the additional stiffness if the tension-stiffening component is included is small. The experimental initial displacement of the experiment is quite large, which could not be simulated. The experimental failure mechanism was rather explosive and caused a complete loss of load-carrying capacity, which can be explained by the brittle behavior of the panel after maximum load. The results of the analysis at a displacement u_h equal to 5 mm [Figs. 10(a and b)] show that the panel is densely cracked with plastic points in the bottom left corner of the panel and in the compressive flange. The results of panel S2 at the ultimate displacement u_h of 15 mm are shown in Figs. 10(c and d) where the redistribution of internal forces in the panel can clearly be observed. The complete loss of stiffness in the bottom of the panel is observed from Fig. 10(d), which is combined with yielding of the reinforcement in compression. The reinforcement in the tension flange also yields, but this is less dominant.

CONCLUSIONS

A simple, phenomenological model has been proposed for finite-element calculations of reinforced-concrete structures. It based on a decomposition of the total stress in a reinforced element into a contribution of the plain concrete, a contribution of the reinforcement, and a contribution that is due to the interaction between concrete and reinforcement. The individual contributions have been formulated using well-established concepts in a rational and consistent manner. The resulting model is robust in the sense that finite-element analyses do not diverge prematurely, and is capable of providing accurate predictions of reinforced-concrete behavior as has been shown by a number of analyses on reinforced-concrete panels and shear walls.

ACKNOWLEDGMENTS

The calculations have been carried out with a pilot version of the DIANA finite-element code. Financial support by the Commission of the European Communities under the Brite-EuRam program (project BE-3275) and by The Netherlands Technology Foundation (grant DCT72.1405) is gratefully acknowledged. The authors wish to thank Jan G. Rots of TNO Building and Construction Research for the stimulating discussions.

APPENDIX. REFERENCES

Bažant, Z. P., and Oh, B. H. (1983). "Crack band theory for fracture of concrete." *Mat. and Struct.*, 93(16), 155–177.

Bhide, S. B., and Collins, M. P. (1987). "Reinforced concrete elements in shear and tension." *Publ. 87-02*, Univ. of Toronto, Toronto, Canada.

de Borst, R. (1986). "Non-linear analysis of frictional materials," PhD thesis, Delft Univ. of Technol., Delft, The Netherlands.

Braam, C. R. (1990). "Control of crack width in deep reinforced concrete beams," PhD thesis, Delft Univ. of Technol., Delft, The Netherlands.

CEB-FIP. (1990). "Model code 1990." *Bulletin d'Information*, Lausanne, Switzerland.

Cervenka, V., Pukl, R., and Eligehausen, R. (1990). "Computer simulation of anchoring technique in reinforced concrete beams." *Computer aided analysis and design of concrete structures*, N. Bićanić et al., eds., Pineridge Press, Swansea, U.K., 1–21.

Crisfield, M. A., and Wills, J. (1989). "Analysis of R/C panels using different concrete models." *J. Engrg. Mech.*, ASCE, 115(3), 578–597.

Feenstra, P. H., and Schellekens, J. C. J. (1992). "Self-adaptive solution algorithm for a constrained Newton-Raphson method." *Rep. 25.2-91-2-13*, Delft Univ. of Technol., Delft, The Netherlands.

Feenstra, P. H. (1993). "Computational aspects of biaxial stress in plain and reinforced concrete," PhD thesis, Delft Univ. of Technol., Delft, The Netherlands.

Hordijk, D. A. (1991). "Local approach to fatigue of concrete," PhD thesis, Delft Univ. of Technol., Delft, The Netherlands.

Isenberg, J. (1993). *Finite element analysis of reinforced concrete structures II*. ASCE, New York, N.Y.

Kollegger, J. (1988). "Ein Materialmodell für die Berechnung von Stahlbetonflächentragwerken," PhD thesis, Gesamthochschule Kassel, Kassel, Germany (in German).

Kollegger, J., and Mehlhorn, G. (1990a). "Experimentelle Untersuchungen zur Bestimmung der Druckfestigkeit des gerissenen Stahlbetons bei einer Querzugbeanspruchung," *Heft 413*, Deutscher Ausschuß für Stahlbeton, Ernst und Sohn, Berlin, Germany (in German).

Kollegger, J., and Mehlhorn, G. (1990b). "Material model for the analysis of reinforced concrete surface structures." *Comp. Mech.*, Vol. 6, 341–357.

Kupfer, H. B., and Gerstle, K. H. (1973). "Behavior of concrete under biaxial stresses." *J. Engrg. Mech.*, ASCE, 99(4), 853–866.
Maier, J., and Thürlimann, B. (1985). "Bruchversuche an Stahlbetonscheiben," *Rep. 8003-1*, Eidgenössische Technische Hochschule, Zürich, Switzerland (in German).
Oliver, J. (1989). "A consistent characteristic length for smeared crack models." *Int. J. Numerical Methods in Engrg.*, Vol. 28, 461–474.
Rots, J. G. (1988). "Computational modeling of concrete fracture," PhD thesis, Delft Univ. of Technol., Delft, The Netherlands.
Rashid, Y. R. (1968). "Analysis of prestressed concrete pressure vessels." *Nuclear Engrg. Des.*, Vol. 7, 334–344.
Suidan, M., and Schnobrich, W. C. (1973). "Finite element analysis of reinforced concrete." *J. Struct. Div.*, ASCE, Vol. 99, 2109–2122.
Vecchio, F. J., and Collins, M. P. (1982). "The response of reinforced concrete to in-plane shear and normal stresses." *Publ. 82-03*, Univ. of Toronto, Toronto, Canada.
Vonk, R. (1992). "Softening of concrete loaded in compression," PhD thesis, Eindhoven Univ. of Technol., Eindhoven, The Netherlands.
Willam, K. (1984). "Experimental and computational aspects of concrete fracture." *Computer aided analysis and design of concrete structures*, N. Bićanić et al., eds., Pineridge Press, Swansea, U.K., 33–70.